Comp. Meth. Civil Eng., Vol. 2, 2 (2011) 127-143

CMCE
Computational Methods in Civil Engineering

Invited Paper

Wave propagation theory in offshore applications

A.M. Kaynia*

Division of Computational Geomechanics, Norwegian Geotechnical Institute (NGI), Oslo, Norway, and

Department of Structural Mechanics, Norwegian University of Science and Technology (NTNU), Trondheim, Norway

Received 5 October 2011

Abstract

A frequency-wavenumber-domain formulation is presented in this paper for calculation of the Green's functions and wave propagation modes in a stratified fluid body underlain by a layered viscoelastic soil medium. The Green's functions define the solid and fluid displacements and fluid pressures due to uniform disk loads acting in either the soil or fluid media. The solution is in the frequency domain and is based on a Fourier expansion of the displacements in the azimuthal direction together with Hankel transform in the radial direction and analytical solutions in the vertical direction. The presented formulation uses the notion of layer stiffness matrices for the solid and fluid layers. Derivation of the expressions for the fluid layer matrices is presented, and a simple procedure for numerical integration of the Green's functions is proposed. Two examples of the use of the presented model are presented. The first example deals with computation of the dynamic impedances of seabed foundations, and the second example concerns computation of fundamental modes of surface waves at the solid-fluid interface. This mode is often used in characterization of the seabed material from the direct seismo-acoustic measurements underwater.

Keywords: Wave propagation; Offshore; Viscoelastic media; Dynamic impedances; Green's functions.

1. Introduction

Within the realm of continuum mechanics, Green's functions are mathematical expressions which define the response of a medium to concentrated loads. Depending on the type of medium, these functions relate displacements or velocities to the applied forces, stresses, dislocations or pressure sources. Although derivations of Green's functions date back long before the computer age, extensive work on their development took off just with the introduction of numerical techniques such as the boundary element methods. A comprehensive coverage of the literature in this subject is beyond the scope of this paper. The reader is referred to classical texts on solid mechanics and wave propagation such as Ewing et al. [1]. Only a few work directly related to this study is cited in the following.

*Corresponding author.
E-mail addresses: amir.m.kaynia@ngi.no (A.M. Kaynia)

Based on the pioneering work of Thomson [2] and Haskell [3], Kausel and Roesset presented a frequency-wavenumber-domain solution for the Green's functions in viscoelastic media [4]. Using a different solution technique, Luco and Apsel presented other expressions for the Green's functions [5]. Both these solutions are based on expanding the load in the horizontal direction and using analytical solutions in the vertical direction. A different approach, reversing the use of analytical and approximate solutions in the two directions, was proposed by Kausel [6] and Waas et al. [7]. These and similar expressions for Green's functions have been incorporated in different applications in earthquake engineering, seismology, site response analyses and seismic site explorations.

Based on the work of Ewing et al. [1] and Kausel and Roesset [4], Stokoe et al. extended the 2-D Green's functions for a layered half-space to include a layer of water over the half-space [8]. They used their results to develop a technique for the inversion of dispersion curve in the surface wave measurements performed offshore. This formulation is extended in this paper to 3-D problems accounting also for layering in the fluid medium. To this end, the solution technique by Kausel and Roesset is adapted to ideal fluid media where the shear modulus is zero (acoustic medium). The derived solutions are in the form of integral expressions. The numerical evaluation of these integrals is implemented in a numerical simulation code from which representative results are calculated for the dynamic impedances of seabed foundations.

Another important application of the developed model is in characterization of offshore sites. Shear modulus is a central parameter in characterizing the mechanical behavior of geo-materials. Low-amplitude shear modulus plays a significant role in such analyses as machine foundation design, site response analyses under seismic excitations, and calculation of foundation impedance in soil-structure interaction studies. In addition, this parameter can be used for characterization of deposits that are hard to sample, such as gravels and cobbles or are difficult to characterize by traditional in situ techniques such as offshore sites. Shear modulus is directly related to the wave velocity of the material. Therefore, an indirect way of estimating the shear modulus is determination of wave velocities, which is often carried out by employing seismic methods.

The commonly used seismic methods for velocity logging in onshore applications are the cross-hole, down-hole and refraction seismic methods. Both the cross-hole and down-hole methods require installation of one or more boreholes. This limits their application offshore. The alternative technique is the surface wave seismic method that is based on measurement of surface waves. Being a noninvasive seismic technique, this method has received more attention recently for onshore and offshore applications. The development in surface wave technique accelerated recently by the introduction of transient excitation (impact) source and implementation of more advanced signal analysis procedures. The technique is commonly known as Spectral Analysis of Surface Waves (SASW) method and is widely used in geodynamic site characterization, construction monitoring, and determination of pavement elastic properties (see, for example, Hiltunen and Gucunski [9]; Tokimatsu [10]; and Haegeman [11]). This method has been extended to offshore applications for site characterization by Stokoe et al. [8] and Luke and Stokoe [12] and detection of gas hydrates by Sedighi-Manesh et al. [13], among others. More recent applications are those by Sauvin et al. [14], Socco et al. [15] and Vanneste et al. [16].

2. Dynamic impedance of foundations on seabed

The technique used here to calculate the impedances is based on the solution proposed by Wong and Luco [17]. According to this technique, the contact surface between the soil and foundation is discretized into a regular grid of rectangular elements. By applying uniformly

distributed unit loads on each element in the three directions and calculating the displacements at all element centers (nodes), one can derive the soil flexibility matrix at the soil/foundation interface. Inversion of this matrix, and imposition of the kinematic conditions for the various response modes of the rigid foundation, leads to computation of the tractions at the soil-foundation interface and determination of the impedances.

This formulation hinges on the availability of a dynamic Green's function for the medium which gives the relationship between the applied loads/tractions and the resulting displacements in the medium. In the present application, the stiffness matrix approach proposed by Kausel and Roësset [4] has been used. Implementation of this method is achieved by assembling layer stiffness matrices and solving the resulting equations for the specified unit forces at layer interfaces. The calculations are carried out under steady-state harmonic vibration at discrete frequencies ω.

The stiffness matrices of the acoustic (fluid) layers are derived in Appendix A of this paper. For the soil layers, the expressions derived by Kausel and Roësset [4] for solid layers have been used in this study. These expressions are summarized in the following for completeness. Appendix A also presents, as example, derivation of the Green's functions for the vertical disk load, and also presents a simple algorithm for their numerical evaluations.

If k denotes the wave number, G is shear modulus, and q and s are defined as

$$q = \sqrt{1-\left(\omega / kV_P\right)^2} \tag{1}$$

$$s = \sqrt{1-\left(\omega / kV_S\right)^2} \tag{2}$$

then the symmetric layer stiffness matrix for the "SV-P wave" case is given by

$$\mathbf{K} = 2\,k\,G\begin{Bmatrix} \mathbf{K}_{11} & \mathbf{K}_{12} \\ \mathbf{K}_{21} & \mathbf{K}_{22} \end{Bmatrix} \tag{3}$$

where

$$\mathbf{K}_{11} = \frac{1-s^2}{2D}\begin{Bmatrix} \frac{1}{s}\left(C^q S^s - qsC^s S^q\right) & -\left(1-C^q C^s + qsS^q S^s\right) \\ -\left(1-C^q C^s + qsS^q S^s\right) & \frac{1}{q}\left(C^s S^q - qsC^q S^s\right) \end{Bmatrix} - \frac{1+s^2}{2}\begin{Bmatrix} 0 & 1 \\ 1 & 0 \end{Bmatrix}$$

$\boldsymbol{K}_{22}$ = same as $\boldsymbol{K}_{11}$, with off-diagonal signs changed

$$\mathbf{K}_{12} = \frac{1-s^2}{2D}\begin{Bmatrix} \frac{1}{s}\left(qsS^q - S^s\right) & -\left(C^q - C^s\right) \\ C^q - C^s & \frac{1}{q}\left(qsS^s - S^q\right) \end{Bmatrix}$$

and the stiffness matrix of the half-space is:

$$\mathbf{K} = 2k\,G\left[\frac{1-s^2}{2(1-qs)}\begin{Bmatrix} q & 1 \\ 1 & s \end{Bmatrix} - \begin{Bmatrix} 0 & 1 \\ 1 & 0 \end{Bmatrix}\right] \tag{4}$$

where

$C^q = \cosh kqh \quad S^q = \sinh kqh$

$C^s = \cosh ksh \quad S^s = \sinh ksh$

$$D = 2\left(1-C^q C^s\right) + \left(\frac{1}{qs} + qs\right) S^q S^s$$

and h is thickness of the layer. The stiffness matrices for a layer and half-space for the "SH-wave" case are

$$\mathbf{K} = \frac{ksG}{\sinh ksh}\begin{Bmatrix} \cosh ksh & -1 \\ -1 & \cosh ksh \end{Bmatrix} \tag{5}$$

$$\mathbf{K} = k\,s\,G \tag{6}$$

Finally, the stiffness matrix of a water layer with free surface is given by (see Appendix A)

$$\mathbf{K}_W = -\frac{\rho\omega^2}{\beta}\begin{bmatrix} \dfrac{\cosh\beta h}{\sinh\beta h} - \dfrac{\beta g}{\omega^2} & -\dfrac{1}{\sinh\beta h} \\ -\dfrac{1}{\sinh\beta h} & \dfrac{\cosh\beta h}{\sinh\beta h} \end{bmatrix} \tag{7}$$

where β is defined as

$$\beta = k\sqrt{1-(\omega/kC)^2} \tag{8}$$

3. Impedances of rigid foundations on seabed

This section presents the vertical impedances of a square foundation with side dimension 2a. Figure 1 shows the geometry and the parameters of the problem under consideration. As expected and verified by previous studies (e.g. Kaynia et al. [18]), the horizontal and rocking impedances are only marginally affected by the presence of the water; therefore, classical solutions for foundations on homogenous half space can be used for them, and this study has focused on vertical response only. The derived impedances are complex quantities which are represented by their real and imaginary parts. For the sake of comparison with other solutions, the vertical impedance is normalized by Ga and its variations with frequency is plotted in terms of the non-dimensional frequency $a_0 = \omega a/V_S$, where G and V_S are the shear modulus and the shear wave velocity of the half space. The presented results are for a hysteretic damping ratio ξ = 0.05. The Green's functions were evaluated by discretizing the soil/foundation interface into a grid of 8x8 elements. Moreover the soil was assumed to have a pressure wave velocity V_P = 1500 m/s (representing typical water-saturated soils)

Figure 2 shows the real and imaginary parts of the normalized vertical impedance of a square foundation. To illustrate the influence of water depth on the impedance, the results are shown for H = 0.0 (no water) to H = 10m. No results are given for higher depths as the impedance practically reached its asymptotic value at H = 10 m. (The dimension of the foundation was 2a = 4m. The water depth beyond which the water has no additional effect on the impedances depends on the foundation dimensions. This is addressed in the following.) Examination of the plots in Figure 2 suggests that the presence of water can be viewed essentially as an added mass-dashpot effect. The added mass is approximately equivalent to the mass of a block of water directly over the foundation with a height of about 0.25a.

The observation that for underwater foundations one could use the corresponding results for foundations on half space with additional damping and mass, has inspired a parametric study to establish practical values for design. To this end, a series of analyses was carried out for a circular foundation with radius a over a uniform half space with different values of Poisson's ratio. The results are presented in Figure 3 in terms of the added damping ratio (left plot) and the height of a

block of water over the foundation normalized by the foundation radius. The latter indicate typically a water height of approximately 25% of the foundation diameter.

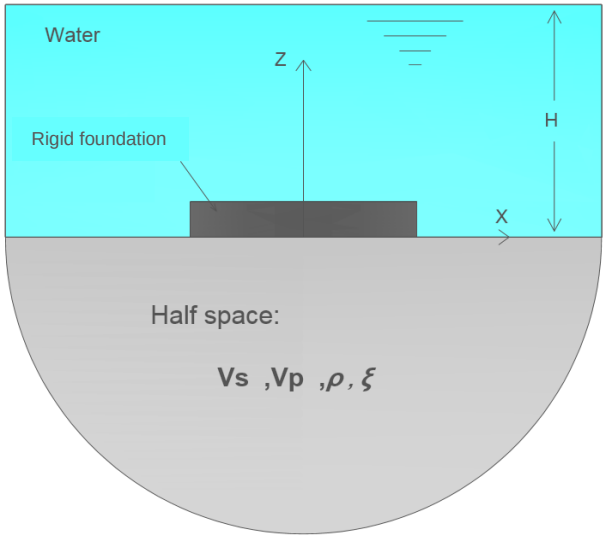

Figure 1. Key elements of soil-water-foundation model used in impedance computations.

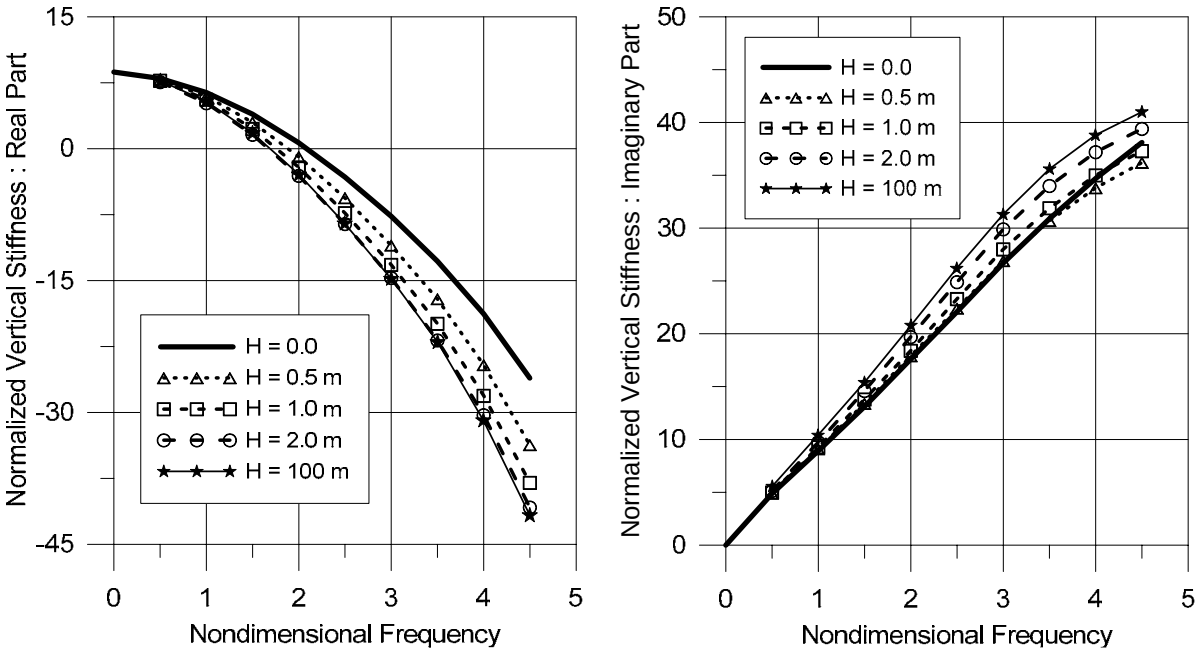

Figure 2. Real and imaginary parts of normalized vertical impedance of rectangular rigid foundation on seabed.

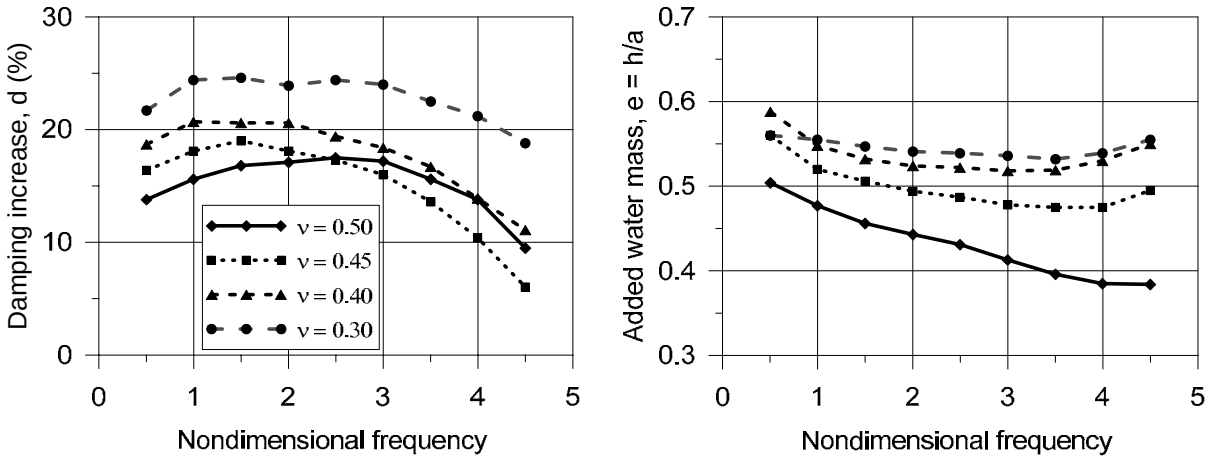

Figure 3. Equivalent mass-damping parameters for circular footing for different values of Poisson's ratio.

4. Numerical simulation of surface wave modes

Measurements of surface wave modes are sometimes used in estimating the soil parameters. The soil profile is often interpreted based on forward modeling algorithms or optimization techniques. Both methods require generation of theoretical dispersion curves for the soil profile. Among the proposed approaches, the one known as the determinant search method [19] has been was adopted in the present study. The procedure is explained in the following, and a number of examples are presented subsequently.

For a layered solid-fluid system, the total stiffness matrix is assembled from the individual layer stiffnesses, in a finite element sense, as described in the previous section. For a given frequency, ω, this matrix is a function of the wave number k. By varying the wave number from an estimated upper bound and calculating the determinant of the total stiffness matrix one can determine the k-values which render the determinant zero. These values, k_i , are the eigenvalues of the problem and correspond to phase velocities $C_i = \omega / k_i$ and wavelengths $\lambda_i = 2\pi/k_i$ of the surface wave modes (Rayleigh wave for onshore and Scholte wave for offshore sites). Alternatively, one could specify the wavelength and vary the phase velocity until a zero determinant is observed. The latter approach has been used in this study. Depending on the soil-fluid parameters, the fundamental mode (as well as other natural modes) can be real or complex. A real mode, which corresponds to a real eigenvalue, k, propagates with in-phase motions of particles in the horizontal and vertical directions. A complex mode, on the other hand, lacks this characteristic and, furthermore, attenuates with distance.

It has been noted earlier (e.g., Stokoe et al. [8]) that in most natural soil deposits, where the soil stiffness increases with depth, the fundamental mode is real. This mode can readily be determined by the determinant search method outlined above. Although a complex mode can also be captured by this method (by allowing the wave number to take on complex values), its implementation for complex cases tends to become inefficient and time consuming [20]. One may expect to encounter complex modes in sites characterized by a stiff layer over softer deposits for wavelengths that span the two contrasting layers. For such sites, the surface wave mode may still be real if the wavelength is too small or too large compared to the thickness of the top layer [21]. To estimate the surface modes for such cases it has become customary in the geophysics community to use only the real part of the determinant. Although this value does not correspond to any realistic physical mode, it has nonetheless

been shown to provide a reasonable estimate of the phase velocity for onshore applications. This approximate approach has been adopted in this study for offshore problems.

A number of case studies are presented in this section to highlight the characteristics of the modes. To this end, three idealized soil profiles were considered. The first is a homogeneous half space. The second one is a profile with increasing stiffness with depth, and the third is a stiff layer over a homogeneous half space. The same mass density, equal to 1800 kg/m^3, and same Poisson's ratio, equal to 0.4, was used in all the soil types. Table 1 gives the shear wave velocities for these soil profiles. In order to study the influence of water on the characteristics of the first surface mode, a range of water heights was considered over each soil profile.

Table 1. Shear wave velocities (in m/s) used for idealized soil profiles.

	Thickness (m)	Profile 1	Profile 2	Profile 3
Layer 1	10	200	100	400
Layer 2	10	200	200	200
Layer 3	10	200	300	200
Half space	∞	200	400	200

Figure 4 displays the calculated dispersion curves of the fundamental Scholte mode in Profiles 1 to 3 for water heights varying from H = 0.0 to H = 70m. The dispersion curves are plotted in the velocity-wavelength domain and cover the wavelength from λ = 5 m to λ = 200 m.

The results for Profile 1 (Figure 4a) show that, as expected, the phase velocity of the fundamental Scholte mode varies between a lower value corresponding to small wavelengths to an upper value corresponding to the first Rayleigh wave mode of the half space (H = 0.0). The lowest Scholte wave velocity in this profile is about 10% lower than that of the Rayleigh wave mode.

Figure 4b illustrates the same set of dispersion curves for Profile 2 (increasing stiffness with depth). The expected gradual increase of phase velocity with wavelength is well reflected by the plots in this figure.

Figure 4c shows the dispersion curves for Profile 3 (stiff layer over softer soil). The mode shapes in this case are complex. It is interesting, however, to observe that the dispersion curve, calculated on the basis of only the real part of the determinant, displays a reasonable pattern from a physical viewpoint. This is true for both the Rayleigh wave mode (H = 0.0) and Scholte modes, although some anomaly is detected for the Rayleigh wave at small λ.

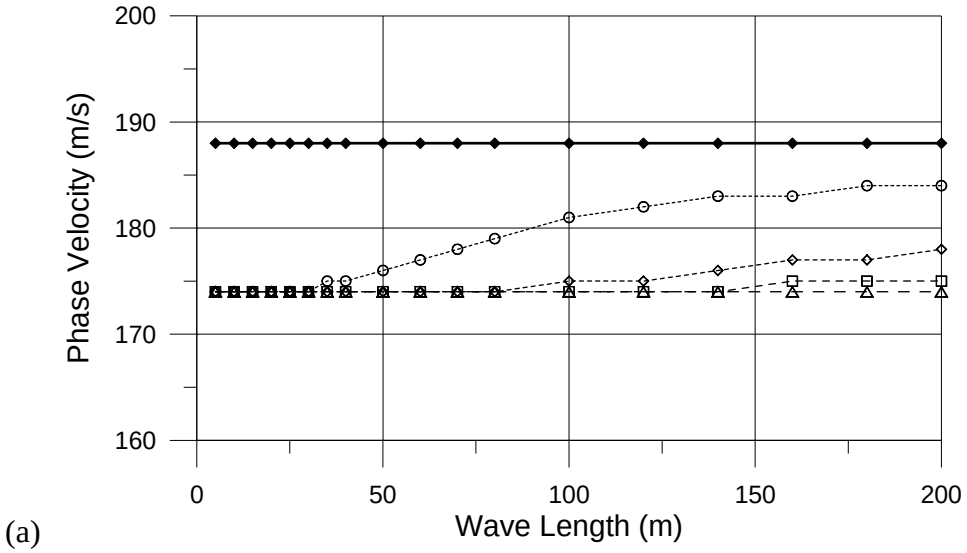

(a)

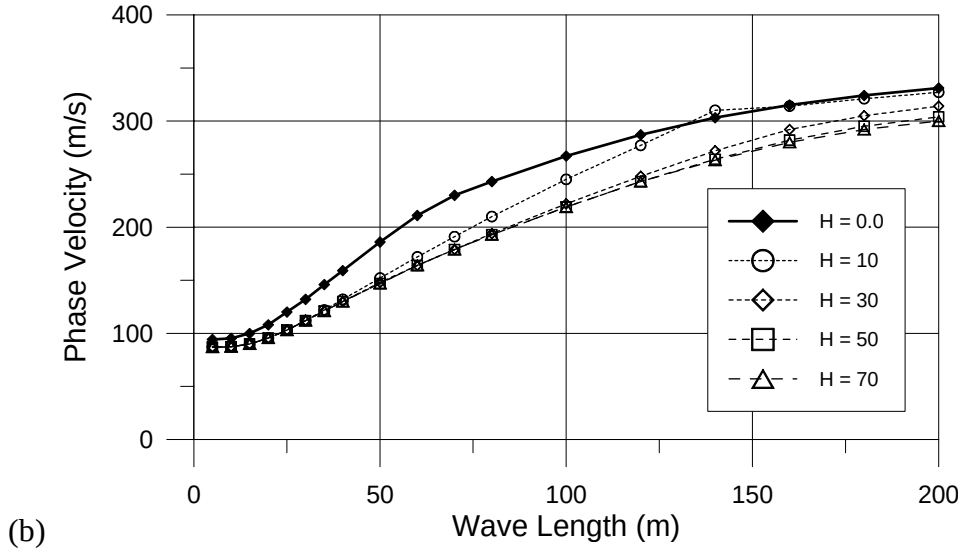

(b)

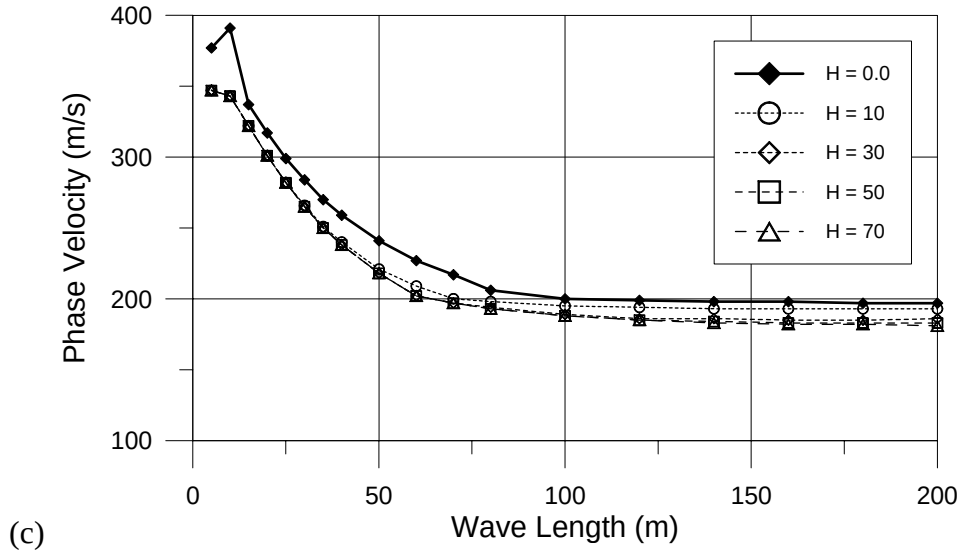

(c)

Figure 4. Dispersion curves of fundamental modes in soil profiles 1, 2 and 3.

To gain more insight into the dynamics of the modes, the fundamental mode shapes in Profile 1 are plotted in Figure 5 for two values of wavelength: 40m (left plot), and 100m (right plot).

The plots display only the normalized vertical components of the fundamental (and the only) mode shape in Profile 1 for four values of water height, H, ranging from 0.0 to 50m. The z-axis points downward with its origin (0.0) at the ground surface; thus, negative z-values correspond to the water layer. Note that as the wavelength increases, the mode shapes corresponding to the various water heights begin to separate.

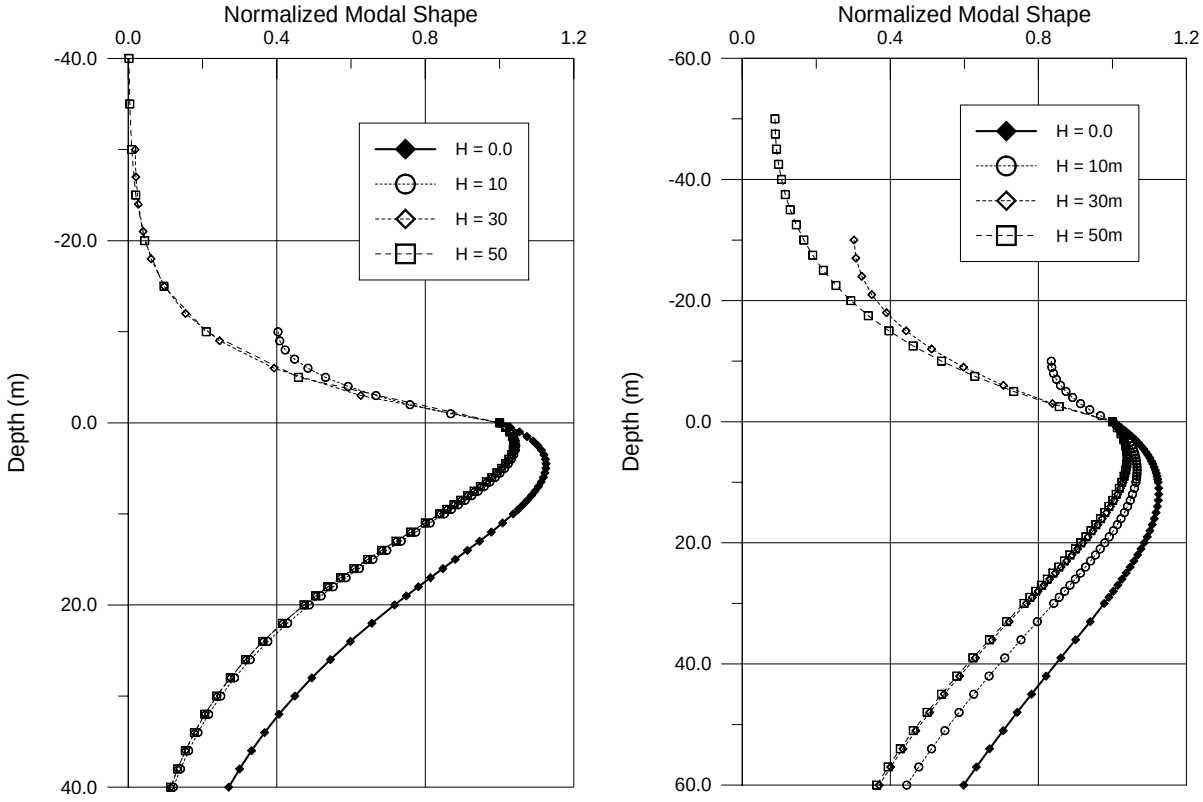

Figure 5. Fundamental mode shape of vertical response in Profile 1 for various water heights: two wavelengths 40m (left) and 100m (right).

5. Summary and conclusions

A frequency-wavenumber-domain formulation was presented in this paper for calculation of the Green's functions and wave propagation modes in a stratified fluid body underlain by a layered viscoelastic soil medium. The formulation is based on the notion of layer stiffness matrices for the solid and fluid layers.

Two examples of the use of the presented model were presented. The first example dealt with computation of the dynamic impedances of seabed foundations, and the second example concerned computation of fundamental modes of surface waves at the solid-fluid interface. This mode is often used in characterization of the seabed material from the direct seismo-acoustic measurements underwater. Numerical results to highlight the use of these results were also presented.

References

[1] W.M. Ewing, W.S. Jardetzky, F. Press, *Elastic waves in layered media*, McGraw-Hill, New York, 1957.

[2] W.T. Thomson, Transmission of elastic waves through a stratified soil medium, *J. Appl. Phys.*, 21 (1950) 89-93.

[3] N.A. Haskell, The dispersion of surface waves on multilayered media, *Bull. Seism. Soc. Am*., 73 (1953) 17-34.

[4] E. Kausel, J.M. Roesset, Stiffness matrices for layered soils, *Bull. Seism. Soc. Am*., Vol.71, 6 (1981) 1743-1761.

[5] J.E. Luco, R.J. Apsel, On the Green's functions for a layered half-space, Part I, *Bull. Seism. Soc. Am*., Vol.73, 4 (1983) 909-929.

[6] E. Kausel, An explicit solution for the Green functions for dynamic loads in layered media, *Report R81-13*, Department of Civil Engineering, MIT, Cambridge, USA, 1981.

[7] G. Waas, H.R. Riggs, H. Werkle, Displacement solutions for dynamic loads in transversely-isotropic stratified media, *Earthquake Eng. Struct. Dynamics*, 13 (1985) 173-193.

[8] K.H. Stokoe II, S.G. Wright, J.M. Roesset, R.C. Gauer, M. Sedighi-Manesh, In-situ measurement of stiffness profiles in ocean-bottom materials using the SASW method, *Proc. Offshore Technology Conference*, OTC paper No. 6234, Houston, Texas, (1990) 299-305.

[9] D.R. Hiltunen, N. Gucunski, Annotated bibliography of SASW method, *Geophysical Characterization of Sites*, R.D. Woods, ed., Special volume of ISSMFE. TC10, New Delhi. Oxford & IBH Publishing Co., (1994) 27-34.

[10] K. Tokimatsu, Geotechnical site characterization using surface waves, *1st. Int. Conf. Earthquake Geotech. Engng., IS-TOKYO '95*, Tokyo, Japan, (1995).

[11] W. Haegeman, Engineering properties of a disposal of dredged sludge covered by cinders, *Proc. Second Int. Conf. Earthquake Geotech. Engng.*, Lisbon, Portugal, (1999).

[12] B.A. Luke, K.H. Stokoe, Application of SASW method underwater, *J. Geotech. & Geoenv. Engng*, Vol.124**,** 6 (1998) 523-531.

[13] M. Sedighi-Manesh, S.G. Wright, J.M. Roësset, K.H. Stokoe, Interpretation of seismic surface wave measurements for detection of gas hydrates offshore, *Proc., Offshore Technology Conference*, OTC paper No. 6852, Houston, Texas, (1992) 369-379.

[14] G. Sauvin, S. Bazin, M. Vanneste, I. Lecomte, A.A. Pfaffhuber, Towards joint inversion/interpretation for landslide-prone areas in Norway - Integrating Geophysics and Geotechnique, Near Surface 2011, *17th European Meeting of Environmental and Engineering Geophysics. EAGE*, Leicester, UK, p. pp. 5. (2011).

[15] V.L. Socco, M. Maraschini, D. Boiero, M. Vanneste, C. Madshus, H. Westerdahl, K. Duffaut, E. Skomedal, On the use of NGI's prototype seabed-coupled shear wave vibrator for shallow soil characterization - Part II: Joint inversion of multi-modal Love and Scholte Surface Waves, *Geophysical Journal International*, 185 (2011) 237-252.

[16] M. Vanneste, C. Madshus, L.V. Socco, M. Maraschini, P.M. Sparrevik, H. Westerdahl, K. Duffaut, E. Skomedal, T.I. Bjørnarå, On the use of NGI's prototype seabed-coupled shear wave vibrator for shallow soil characterization - Part I: Acquisition and processing of surface waves, *Geophysical Journal International*, 185 (2011) 221-236.

[17] H.L. Wong, J.E. Luco, Dynamic response of rigid foundations of arbitrary shape, *Earthquake Engrg. Struct. Dyn*., 4 (1976) 579-587.

[18] A.M. Kaynia, E. Kausel, C.M. Madshus, Impedances of Underwater Rigid Square Foundations, *Proc. ASCE Spec. Conf. Geotech. Earthquake Engng*, Seattle, WA, USA, (1998) 1283–1293.

[19] S. Nazarian, K.H. Stokoe, In situ shear wave velocities from spectral analysis of surface waves, *Proc. Eighth World Conf. on earthquake Engng*., San Francisco, USA, Vol. III, (1984) 31-38.

[20] B. Lee, Analytical studies of surface wave propagation along the seafloor for application to spectral-analysis-of-surface-waves (SASW) testing, *Res. Rep., Offshore Technology Research Center*, Univ. of Texas at Austin, USA, 1996.

[21] J.M. Roësset, D.W. Chang, K.H. Stokoe, M. Aouad, Modulus and thickness of the pavement surface layer from SASW tests, *Transportation Research Record*, 1260 (1989) 53-63.

Appendix-A: Derivation of Green's functions in acoustic layers

This section presents the mathematical formulation for the problem of wave propagation in layered solids under water. It begins with the governing differential equations in both solid and acoustic media, then proceeds to the development of stiffness matrices for the layers, and finally presents integral solutions for the Green's functions. Both a limited-depth acoustic layer and half-space acoustic medium are considered. The derivations are carried out under steady-state harmonic conditions. Therefore all variables have time variations of the form $A(r, t) = \overline{A}(r)\, e^{i\omega t}$, where r represents space variables, t denotes time and ω is the frequency. The response to an arbitrary loading function is then achieved through a Fourier synthesis of harmonic solutions.

If the displacements in the radial, tangential and vertical directions in a solid or acoustic medium are denoted by u_r, u_θ and u_z, respectively, and the corresponding external loads per unit volume are f_r, f_θ and f_z, the differential equations of wave propagation in an elastic solid or acoustic medium can be expressed as

$$(\lambda+2\mu)\frac{\partial \Delta}{\partial r}-\frac{2\mu}{r}\frac{\partial \omega_z}{\partial \theta}+2\mu\frac{\partial \omega_\theta}{\partial z}+\omega^2\rho u_r+f_r=0 \tag{A1-a}$$

$$(\lambda+2\mu)\frac{1}{r}\frac{\partial \Delta}{\partial \theta}-2\mu\frac{\partial \omega_r}{\partial z}+2\mu\frac{\partial \omega_z}{\partial r}+\omega^2\rho u_\theta+f_\theta=0 \tag{A1-b}$$

$$(\lambda+2\mu)\frac{\partial \Delta}{\partial z}-\frac{2\mu}{r}\frac{\partial}{\partial r}(r\omega_\theta)+\frac{2\mu}{r}\frac{\partial \omega_r}{\partial \theta}+\omega^2\rho u_z+f_z=0 \tag{A1-c}$$

where λ and μ are Lamé constants, and ρ is the mass density. The dilatation Δ and the rotations ω_r, ω_θ and ω_z are given by:

$$\Delta=\frac{1}{r}\frac{\partial}{\partial r}(ru_r)+\frac{1}{r}\frac{\partial u_\theta}{\partial \theta}+\frac{\partial u_z}{\partial z} \tag{A2}$$

$$\omega_r=\frac{1}{2}\left[\frac{1}{r}\frac{\partial u_z}{\partial_\theta}-\frac{\partial u_\theta}{\partial z}\right] \tag{A3-a}$$

$$\omega_\theta=\frac{1}{2}\left[\frac{\partial u_r}{\partial_z}-\frac{\partial u_z}{\partial r}\right] \tag{A3-b}$$

$$\omega_z=\frac{1}{2r}\left[\frac{\partial}{\partial r}(ru_\theta)-\frac{\partial u_r}{\partial \theta}\right] \tag{A3-c}$$

In the following derivations it is assumed that the acoustic medium is an ideal fluid with zero shear modulus and, thus, no shear stress, and the external (body) sources are zero; that is, $f_r = f_\theta = f_z = 0$. The sources are then considered as surface tractions at layer interfaces or point sources in the acoustic medium. This assumption does not impose any practical restriction on the model, but makes derivations and the code development more straightforward.

To solve equation (A1), one may expand displacements in Fourier series in tangential direction as

$$\begin{Bmatrix} u_r(r,\theta,z) \\ u_z(r,\theta,z) \end{Bmatrix}=\sum_{n=0}^{\infty}\begin{Bmatrix} u_{rn}(r,z) \\ u_{zn}(r,z) \end{Bmatrix}\cos n\theta \tag{A4}$$

$$u_\theta(r,\theta,z)=\sum_{n=0}^{\infty}u_{\theta n}(r,z)\sin n\theta$$

It is necessary at this point to differentiate between the solutions in the solid continuum and the acoustic medium. The solution for the former has been obtained by Kausel and Roesset [4] and, therefore, is not repeated there. However, the final results, in the form of the stiffness matrices of layers, will are included in the main text of this paper for convenience of reference. The same solution technique proposed by Kausel and Roesset [4] was pursued here for obtaining the stiffness matrices for acoustic layers. The details are given in the following sections.

Solution of acoustic equations

Setting $\mu = 0$ in equation (A1) and substituting relations (A4) in equation (A1) to (A3) one obtains:

$$\sum_0^\infty \left(\lambda \frac{\partial \Delta_n}{\partial r} + \omega^2 \rho u_{rn} \right) \cos n\theta = 0 \tag{A5-a}$$

$$\sum_0^\infty \left(-\lambda \frac{n}{r} \Delta_n + \omega^2 \rho u_{\theta n} \right) \sin n\theta = 0 \tag{A5-b}$$

$$\sum_0^\infty \left(\lambda \frac{\partial \Delta_n}{\partial z} + \omega^2 \rho u_{zn} \right) \cos n\theta = 0 \tag{A5-c}$$

where

$$\Delta_n = \frac{1}{r} \frac{\partial}{\partial r} (r u_{rn}) + \frac{n}{r} u_{\theta n} + \frac{\partial u_{zn}}{\partial z} \tag{A6}$$

In order that the above equations are satisfied, it is necessary that the terms in the parentheses are identically zero. Then combination of equation (A5-a) and (A5-b) leads to the following three equations, to be satisfied by any value of n:

$$\lambda \left(\frac{\partial \Delta_n}{\partial r} - \frac{n}{r} \Delta_n \right) + \omega^2 \rho (u_{rn} + u_{\theta n}) = 0 \tag{A7-a}$$

$$\lambda \left(\frac{\partial \Delta_n}{\partial r} + \frac{n}{r} \Delta_n \right) + \omega^2 \rho (u_{rn} - u_{\theta n}) = 0 \tag{A7-b}$$

$$\lambda \frac{\partial \Delta_n}{\partial z} + \omega^2 \rho u_{zn} = 0 \tag{A7-c}$$

Defining now the following Hankel transforms:

$$u_{1n}(k,z) + u_{3n}(k,z) = \int_0^\infty (u_{rn} + u_{\theta n}) J_{n+1}(kr) r dr \tag{A8-a}$$

$$-u_{1n}(k,z) + u_{3n}(k,z) = \int_0^\infty (u_{rn} - u_{\theta n}) J_{n-1}(kr) r dr \tag{A8-b}$$

$$u_{2n}(k,z) = \int_0^\infty u_{zn} J_n(kr) r dr \tag{A8-c}$$

where $J_n(kr)$ is the n[th] order Bessel function of the *1st* kind and k the radial wave number, and using the following properties of Bessel functions

$$\int_0^\infty \left[\frac{\partial^2}{\partial r^2} + \frac{1}{r} \frac{\partial}{\partial r} - \frac{m^2}{r^2} + \frac{\partial^2}{\partial z^2} \right] \varphi J_m(kr) r dr = \left(\frac{d^2}{dz^2} - k^2 \right) \int_0^\infty \varphi J_m(kr) r dr$$

$$\int_0^\infty \left[\frac{d}{dr}-\frac{m}{r}\right]\varphi J_{m+1}(kr)r\,dr=-k\int_0^\infty \varphi J_m(kr)r\,dr \tag{A9}$$

$$\int_0^\infty \left[\frac{d}{dr}+\frac{m}{r}\right]\varphi J_{m-1}(kr)r\,dr=k\int_0^\infty \varphi J_m(kr)r\,dr$$

one can show that Hankel transform of equation (A7) leads to

$$-k\lambda\Delta'_n+\rho\omega^2\left(u_{1n}+u_{3n}\right)=0 \tag{A10-a}$$

$$k\lambda\Delta'_n+\rho\omega^2\left(-u_{1n}+u_{3n}\right)=0 \tag{A10-b}$$

$$\lambda\frac{d}{dz}\Delta'_n+\rho\omega^2 u_{2n}=0 \tag{A10-c}$$

where $\Delta'_n=\int_o^\infty \Delta_n J_n(kr)r\,dr=ku_{1n}+\frac{d}{dz}u_{2n}$. Introducing this relation in equation (A10), one can derive the following equations:

$$u_{3n}=0 \quad n=0,1,2\ldots..\infty \tag{A11}$$

$$\left(-k^2\lambda+\rho\omega^2\right)u_{1n}-\lambda k\frac{d}{dz}u_{2n}=0 \tag{A12-a}$$

$$(\lambda k)\frac{d}{dz}u_{1n}+\left[\lambda\frac{d^2}{dz^2}+\rho\omega^2\right]u_{2n}=0 \tag{A12-b}$$

Finally, substituting from equation (A12-a) for u_{1n} in equation (A12-b) one gets:

$$\frac{d^2}{dz^2}u_{2n}+\frac{\rho\omega^2-\lambda k^2}{\lambda}u_{2n}=0 \tag{A13}$$

which can also be expressed as

$$\frac{d^2}{dz^2}u_{2n}-\beta^2 u_{2n}=0 \tag{A14}$$

where

$$\beta=\left(k^2-\frac{\rho\omega^2}{\lambda}\right)^{1/2}=\left(k^2-\frac{\omega^2}{C_b^2}\right)^{1/2} \tag{A15}$$

and $C_b=(\lambda/\rho)^{1/2}$ is the speed of sound in the fluid.

Solving equation (A14) for u_{2n} and substituting in equation (A12-a) for u_{1n} one obtains the following solutions:

$$u_{2n}=Ae^{\beta z}+Be^{-\beta z} \tag{A16-a}$$

$$u_{3n}=0 \tag{A16-b}$$

$$u_{1n}=-\frac{k}{\beta}\left[Ae^{\beta z}-Be^{-\beta z}\right] \tag{A16-c}$$

where *A* and *B* are unknown constants.

Stiffness matrices for acoustic layer

To derive the stiffness matrix of an acoustic layer, similar to the derivations by Kausel and Roesset [4], for an elastic solid layer, one has to develop expressions for the stresses.

The only nonzero component of stress in an acoustic medium, on a plane perpendicular to the Z-axis, is σ_{zz} which is given by

$$\sigma_{zz} = \lambda \Delta \tag{A17}$$

using the displacement expansions in (A4) and Δ given by equation (A2), one can derive the following expression for the vertical normal stress:

$$\sigma_{zz} = \sum_{0}^{\infty} \sigma_{zzn} \cos n\theta \tag{A18}$$

where

$$\sigma_{zzn} = \lambda \frac{\partial u_{zn}}{\partial z} + \lambda \left(\frac{\partial u_{rn}}{\partial r} + \frac{u_{rn}}{r} + \frac{n}{r} u_{\theta n} \right) \tag{A19}$$

Defining now the following Hankel transform of the stress

$$\sigma_{22n}(k, z) = \int_0^{\infty} \sigma_{zzn} J_n(kr) r dr \tag{A20}$$

one can show that

$$\sigma_{22n} = \lambda \left(\frac{du_{2n}}{dz} + k u_{1n} \right) \tag{A21}$$

Substituting for u_{1n} and u_{2n} from equation (A16) in equation (A21) one gets

$$\sigma_{22n} = \frac{\rho \omega^2}{\beta} \left[-A e^{\beta z} + B e^{-\beta z} \right] \tag{A22}$$

For an acoustic layer of thickness *h* (Figure 1b) one can use equation (A16-a) to express u^{0}_{2n} and u^{-h}_{2n} at the top ($z = 0$) and bottom ($z = -h$) of the layer as a function of A and B and, at the same time, use equation (A22) to express fluid pressures $p^{0}_{2n} = \sigma^{0}_{22n}$ and $p^{-h}_{2n} = -\sigma^{-h}_{22n}$ at the top and bottom of the layer in terms of A and B. Elimination of the unknowns *A* and *B* from the resulting four equations leads to the following relations:

$$p^{0}_{2n} = -\frac{\rho \omega^2}{\beta} \left[\frac{\cosh \beta h}{\sinh \beta h} u^{0}_{2n} - \frac{1}{\sinh \beta h} u^{-h}_{2n} \right] \tag{A23-a}$$

$$p^{-h}_{2n} = -\frac{\rho \omega^2}{\beta} \left[\frac{1}{\sin \beta h} u^{0}_{2n} - \frac{\cosh \beta h}{\sinh \beta h} u^{-h}_{2n} \right] \tag{A23-b}$$

which can be expressed in matrix form as

$$\begin{Bmatrix} p^{0}_{2n} \\ p^{-h}_{2n} \end{Bmatrix} = -\frac{\rho \omega^2}{\beta \sinh \beta h} \begin{bmatrix} \cosh \beta h & -1 \\ -1 & \cosh \beta h \end{bmatrix} \begin{Bmatrix} u^{0}_{2n} \\ u^{-h}_{2n} \end{Bmatrix} \tag{A24}$$

The stiffness matrix of the acoustic layer is then the matrix which multiplies the displacement vector in equation (A24).

In addition to the general stiffness matrix of the layer, one needs to consider one of the following two cases, depending on the extent of the acoustic medium.

a) Acoustic half-space

For this case, both u and p approach zero as $z \to \infty$. Therefore, one should have $A = 0$ in equation (A16-a) and (A22). Eliminating B from these equations and expressing the stress versus the displacement, one gets

$$p_{2n}^{H} = -\frac{\rho\omega^2}{\beta} u_{2n}^{H} \tag{A25}$$

where the superscript H is used to denote "half space". In this case the stiffness matrix reduces to a scalar.

b) Layer with free surface

For the free surface, the condition at a point on this surface is

$$p_a = 0 = p_b - \rho g u_z \tag{A26}$$

That is $p_b^0 = \rho g u_z^0 . Since\ p = -\sigma_{zz}, one\ has \sigma_{zz}^0 = -\rho g u_z^0 \ and\ thus \sigma_{22n}^0 = -\rho g u_{2n}^0 .$ Therefore, one obtains

$$p_{2n}^0 = \sigma_{22n}^0 = -\rho g u_{2n}^0 \tag{A27}$$

Introducing this relation in the stiffness expression of the layer, equation (A24), one can derive the stiffness matrix of an acoustic layer with free surface, as

$$\begin{Bmatrix} 0 \\ p_{2n}^{-h} \end{Bmatrix} = -\frac{\rho\omega^2}{\beta} \begin{bmatrix} \dfrac{\cosh\beta h}{\sinh\beta h} - \dfrac{\beta g}{\omega^2} & -\dfrac{1}{\sinh\beta h} \\ -\dfrac{1}{\sinh\beta h} & \dfrac{\cosh\beta h}{\sinh\beta h} \end{bmatrix} \begin{Bmatrix} u_{2n}^0 \\ u_{2n}^{-h} \end{Bmatrix} \tag{A28}$$

Integral representation of Green's functions

The first step in deriving the Green's functions is to calculate the transformed displacements u_{1n} and u_{2n} for applicable values of *n*. This is achieved by assembling the stiffness matrices of the solid and acoustic layers, as in a traditional finite element method, and solving for the interface displacements, u_{1n} and u_{2n}, under the specified interface forces. This operation requires the transformed forces for a given stress condition. The details of such a derivation are outlined here for the case of a uniform vertical load over a circular disk at the solid-fluid interface. This is a case frequently encountered in various applications of under-water seismic. The derivations for other cases can simply follow the principles presented here.

For a vertical unit load over a circular disk with radius R, one has the following stress conditions:

$$\begin{cases} \bar{\sigma}_{rz} = \bar{\sigma}_{\theta z} = 0 \\ \qquad\qquad r \le R \\ \bar{\sigma}_{zz} = \dfrac{1}{\pi R^2} \end{cases} \tag{A29-a}$$

$$\bar{\sigma}_{rz} = \bar{\sigma}_{\theta z} = \bar{\sigma}_{zz} = 0; r > R \tag{A29-b}$$

where overbar is used to differentiate the applied stresses from the internal stresses. If a Fourier transform of the load (as in equation A18), is compared with equation (A29) one can observe that

$$\begin{aligned} &\bar{\sigma}_{rz0} = \bar{\sigma}_{\theta z0} = 0 \\ &\bar{\sigma}_{zz0} = \frac{1}{\pi R^2} \\ &\bar{\sigma}_{rzn} = \bar{\sigma}_{\theta zn} = \bar{\sigma}_{zzn} = 0; n \ge 1 \end{aligned} \tag{A30}$$

This means that the displacements are only contributed by the terms associated with n = 0. Therefore the displacement expansions reduce to the following expressions:

$$u_r(r, \theta, z) = u_{ro}(r, z) \tag{A31-a}$$

$$u_\theta(r, \theta, z) = 0 \tag{A31-b}$$

$$u_z(r, \theta, z) = u_{zo}(r, z) \tag{A31-c}$$

Applying Hankel transform to the stresses given in equation (A30) one gets (see equation A20)

$$\bar{\sigma}_{220} = \frac{1}{\pi R^2}\int_0^R J_0(kr) r dr = \frac{1}{\pi}\frac{J_1(kR)}{kR} \tag{A32}$$

Therefore, if the stiffness relation for a medium is solved for a unit load at a given interface and the resulting transformed displacements at a desired point are denoted as $\bar{u}_{10} and\ \bar{u}_{20}$ then, from equation (A8), one can write (note that although the stiffness matrices of acoustic layers involve only u_2, the solid/fluid ensemble retains both u_1 and u_2)

$$\frac{1}{\pi}\frac{J_1(kR)}{kR}\bar{u}_{10} = \int_0^\infty (u_{ro}) J_1(kr) r dr \tag{A33-a}$$

$$\frac{1}{\pi}\frac{J_1(kR)}{kR}\bar{u}_{20} = \int_0^\infty (u_{zo}) J_0(kr) r dr \tag{A33-b}$$

Finally, taking inverse Hankel transform of these expressions, one obtains the following integral representations for the vertical and radial displacements (that is, the Green's functions):

$$u_{ro}(r, z) = \frac{1}{\pi}\int_0^\infty \bar{u}_{10} J_1(kr)\frac{J_1(kR)}{kR} k dk \tag{A34-a}$$

$$u_{zo}(r, z) = \frac{1}{\pi}\int_0^\infty \bar{u}_{20} J_0(kr)\frac{J_1(kR)}{kR} k dk \tag{A34-b}$$

The calculation of pressures at layer interfaces is straightforward. To this end, having calculated the transformed displacements at layer interfaces, one may simply use the stiffness relationship in the pertinent layer and calculate the transformed pressures. The pressures can then be derived from inverse transformations similar to equation (A34). For instance, if $\bar{P}$ is an

interface transformed pressure due to a unit vertical disk load, one can show that the pressure at any point along that interface would be

$$p(r,z)=\frac{1}{\pi}\int_0^{\infty} \bar{p}\, J_0(kr)\frac{J_1(kR)}{kR}\,kdk \qquad \text{(A35)}$$

Numerical evaluation of integrals

The above integrals have to be evaluated numerically. For this purpose, one needs to use a scheme to make sure that the sharp peaks in the variation of the integrands are captured within the Δk used for the numerical integration. A rigorous scheme has been proposed by Apsel and Luco [5]. It takes advantage of locating the sharp peaks in the integrand in establishing a sufficiently small Δk and the asymptotic expansions of the Bessel functions for large k-values. One could also adopt a simple integration procedure and obtain fairly accurate results if one carefully selects Δk in the integration region and take advantage of the exponentially decaying properties of the integrands.

A potential source of inaccuracy is the truncation of the integrals at some cutoff wave number which results in an artificial spatial periodicity of the load. If N denotes the number of integration steps, then $L = 2RN$ would be the spatial period of the load. The integration step can be taken as $\Delta k = 2\pi/L$ and the cutoff wave number (Nyquist wave number) would then be equal to $k_{max} = N\,\Delta k$. For a given frequency, ω, the selected N and Δk should be such that $k_{max} > 2\omega/V_{S,min}$, where $V_{S,min}$ is the smallest shear wave velocity in the soil profile. The reason for this restriction is that the integrands are highly wavy below k_{max} while above this value they decay either uniformly or exponentially with wave number, depending on the elevation distance between the observation and source points.